Monthly Notices
of the
ROYAL ASTRONOMICAL SOCIETY

Mon. Not. R. Astron. Soc. **406,** 1944–1958 (2010) doi:10.1111/j.1365-2966.2010.16787.x

The luminosity function and the rate of *Swift*'s gamma-ray bursts

David Wanderman⋆ and Tsvi Piran⋆

Racah Institute of Physics, The Hebrew University, Jerusalem 91904, Israel

Accepted 2010 April 7. Received 2010 March 8; in original form 2009 December 3

ABSTRACT

We invert directly the redshift–luminosity distribution of observed long *Swift* gamma-ray bursts (GRBs) to obtain their rate and luminosity function. Our best-fitting rate is described by a broken power law that rises like $(1+z)^{2.1^{+0.5}_{-0.6}}$ for $0 < z < 3$ and decreases like $(1+z)^{-1.4^{+2.4}_{-1.0}}$ for $z > 3$. The local rate is $\rho_0 \simeq 1.3^{+0.6}_{-0.7}$ (Gpc^{-3} yr^{-1}). The luminosity function is well described by a broken power law with a break at $L* \simeq 10^{52.5\pm0.2}$ (erg s^{-1}) and with indices $\alpha = 0.2^{+0.2}_{-0.1}$ and $\beta = 1.4^{+0.3}_{-0.6}$. The recently detected GRB 090423, with $z \approx 8$, fits nicely into the model's prediction, verifying that we are allowed to extend our results to high redshifts. While the GRB rate may follow the star formation rate (SFR) for $z < 3$, the high-redshift slope is shallower than the steep decline in the SFR for $4 < z$. However, we cannot rule out a GRB rate that follows one of the recent SFR models.

Key words: gamma-ray burst: general – stars: formation.

1 INTRODUCTION

Gamma-ray bursts (GRBs) are short and intense pulses of soft gamma-rays. In this work, we study their luminosity function and their cosmic rate. These functions are essential to understand the nature of GRBs and to determine their progenitors. They may also shed light on the still mysterious physics of the central engine.

The luminosity function and the cosmic GRB rate are observationally entangled as the observed rate is a convolution of the luminosity function with the cosmic rate. For this reason, almost every work before this paper has made an a priori assumption on at least one of these functions. At first – having no motivation to believe otherwise – the rate was assumed to be constant. The simplest form for the luminosity function was a standard candle i.e. a constant luminosity. These early studies used the measured $\langle V/V_{\rm max}\rangle$ value to find the typical luminosity (Mao & Paczynski 1992; Piran 1992; Fenimore et al. 1993; Ulmer & Wijers 1995; Ulmer, Wijers & Fenimore 1995) and correspondingly a maximal distance from which GRBs were observed. Later, using the flux distribution ($\log N$–$\log P$ relation), Cohen & Piran (1995) and Loredo & Wasserman (1998) showed how relaxing the standard candle assumption allows a corresponding relaxation of the constant rate assumption.

Paczyński (1998) noted that the hosts of the bursts are in star-forming regions and suggested that GRBs follow the star formation rate (SFR) (see also Totani 1997; Wijers et al. 1998). The detection of a supernova associated with GRB 980425 (Galama et al. 1998), strengthened the expectation that the GRB rate should follow the SFR. Using this proportionality, numerous studies examined the typical luminosity assuming at first standard candles (e.g. Wijers et al. 1998; Totani 1999) and later more elaborate shapes of the luminosity function (e.g. Schmidt 1999, 2001a,b; Firmani et al. 2004; Guetta & Piran 2005; Guetta, Piran & Waxman et al. 2005).

Swift, which discovers routinely GRBs afterglows, detected GRBs from higher redshifts than was previously possible sparked renewed interest in the GRB redshift distribution (e.g. Berger et al. 2005; Natarajan et al. 2005; Bromm & Loeb 2006; Jakobsson et al. 2006; Chary, Berger & Cowie 2007; Le & Dermer 2007; Liang et al. 2007; Salvaterra & Chincarini 2007; Yüksel & Kistler 2007). More and more signs appeared suggesting that the rate of GRBs does not simply follow the global SFR, as was believed earlier. Firmani et al. (2005), Le Floc'h et al. (2006), Daigne, Rossi & Mochkovitch (2006), Le & Dermer (2007) and Guetta & Piran (2007) conclude that the GRB rate differs from the SFR. In particular, we observe more high-redshift bursts than what is expected for a rate that follows the SFR. Yüksel et al. (2008) uses the high-luminosity subsample of bursts to obtain the GRB rate without assuming any luminosity function. They find that the GRB rate at high redshifts ($z > 4$) is higher than Hopkins & Beacom (2006) SFR. Alternatively, luminosity evolution has been suggested by some authors (e.g. Lloyd-Ronning, Fryer & Ramirez-Ruiz 2002; Firmani et al. 2004; Matsubayashi et al. 2005; Kocevski & Liang 2006). Salvaterra et al. (2008) used a sample of long bursts with redshift and found evidence for luminosity evolution. Other papers, including this one, find self-consistency without a luminosity evolution.

We introduce here a new method for determining the rate and the luminosity, by inverting the observations without making any assumptions on the functional form of the luminosity and rate functions. This direct inversion allows us to use most of the available redshift data and to obtain robust estimation of both functions.

⋆E-mail: david.wanderman@mail.huji.ac.il (DW); tsvi@phys.huji.ac.il (TP)

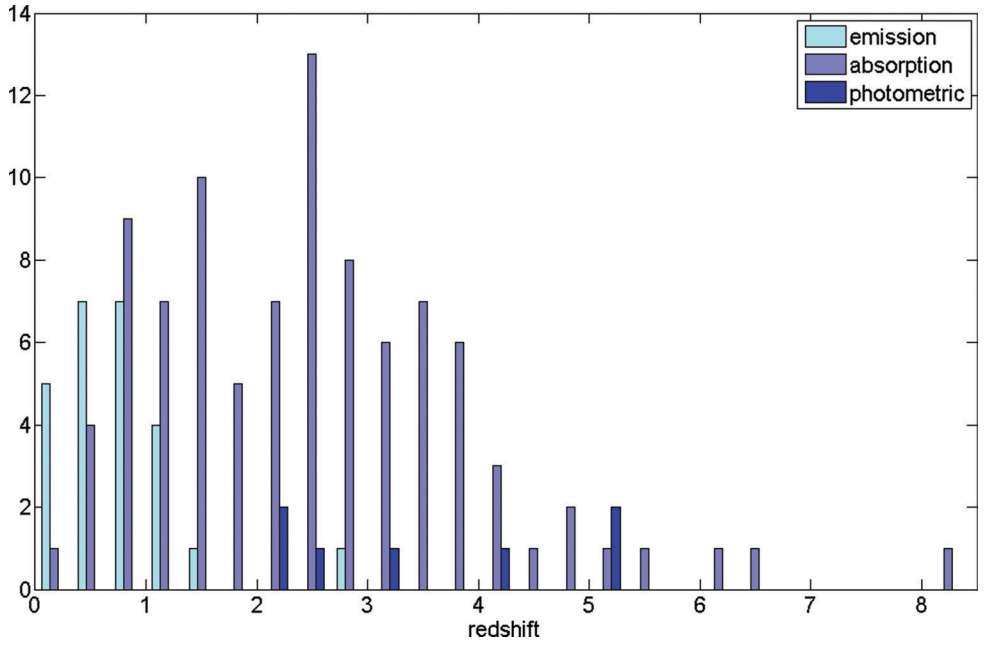

Figure 1. The redshift distribution for the different methods: absorption lines, emission lines and photometry.

In Section 2, we describe the subsample of bursts we analyse and its advantages over other samples. In Section 3, we introduce a new formalism allowing us to directly invert the observed distribution and obtain the intrinsic luminosity function and rate. In Section 4, we present the results obtained using this method and the confidence ranges associated with them. In Section 5, we address the question whether the GRB rate is consistent with the SFR. We discuss a few implications of the results in Section 6.

2 THE SAMPLE

We consider long bursts ($t_{90} \geq 2$ s) detected by *Swift* from the beginning of its operation until burst 090726,[1] with a measured peak flux and a measured redshift. Generally, GRBs redshifts are obtained from the optical afterglow spectrum using absorption lines or photometry, or from the spectrum of the host galaxy using emission lines. However in the global sample, we find different redshift distributions for the different detection methods namely: absorption, emission and photometry (see Fig. 1). For redshifts determined using the hosts' emission lines, we do not detect high-redshift events, whereas absorption lines redshifts extend over the entire range of redshifts. Furthermore, emission lines are more susceptible to a selection effect known as the 'redshift desert' in the range $1.1 < z < 2.1$,[2] (Fiore et al. 2007, see also Coward 2008). This is in line with the fact that we have also found that the probability to measure the redshift using emission lines strongly depends on the gamma-ray flux, favouring high fluxes.[3] This effect is mild for absorption lines and photometry (see Appendix B).

To obtain a more uniform sample, we consider therefore only bursts whose redshift was measured using the afterglow. For each burst we calculate the isotropic equivalent peak luminosity: $L_{\rm iso}$ (see Appendix A, for details) using the peak flux and redshift. We use standard Λ cold dark matter cosmology with $h = 0.7, \Omega_{\rm m} = 0.27, \Omega_\Lambda = 0.73$.

3 A DIRECT ESTIMATE OF THE LUMINOSITY FUNCTION AND THE RATE

3.1 Assumptions

We assume that the luminosity function is redshift independent. In this case, the number of bursts at a given redshift and with a given luminosity is the product of the luminosity function, $\phi(L)$, that depends only on the luminosity L and the GRB rate, $R_{\rm GRB}(z)$, that depends only on the redshift z. This common assumption is reasonable since a priori there is no competing reason why the luminosity function should depend on the redshift. We test later the validity of this assumption and show that it is accepted with a high statistical significance.

The isotropic peak luminosity function, $\phi(L)$, is defined traditionally as the fraction of GRBs with isotropic equivalent luminosities in the interval $\log L$ and $\log L + {\rm d}\log L$. The rate, $R_{\rm GRB}(z)$, is defined as the comoving space density of GRBs in the interval z to $z + {\rm d}z$. The distribution density, $n(L, z)$ is given by

$$n(L, z)\,{\rm d}\log L\,{\rm d}z = \phi(L)R(z)\,{\rm d}\log L\,{\rm d}z, \quad (1)$$

where

$$R(z) = \frac{R_{\rm GRB}(z)}{(1+z)}\frac{{\rm d}V(z)}{{\rm d}z} \quad (2)$$

is the differential comoving rate of bursts at a redshift z, ${\rm d}V(z)/{\rm d}z$ is the derivative of the volume element and the factor $(1 + z)^{-1}$ reflects the cosmological time dilation.

3.2 Formalism

We consider now a direct method to invert the observed L–z distribution and obtain the functions ϕ and $R_{\rm GRB}$. To do so, we approximate

[1] All data were taken from the *Swift* information page http://swift.gsfc.nasa.gov/docs/swift/archive/grb_table/.

[2] Although a redshift determination through absorption lines is also difficult in the range $1.5 < z < 2.1$.

[3] A possible explanation is that a brighter burst can be more easily localized, making follow-up possible.

$\phi(L)$ and $R(z)$ as *step functions* whose range is divided into bins with a constant value within each bin. These functions can be expressed as a sum of Heaviside functions.

First, we divide both luminosity and redshift intervals into bins. We denote

$$\phi_i \equiv \phi(L_i \le L < L_{i+1}) \,, \tag{3}$$

$$\begin{aligned} R_j &\equiv R(z_j \le z < z_{j+1}) \\ &= \frac{1}{(z_{j+1}-z_j)} \int_{z_j}^{z_{j+1}} \mathrm{d}z \frac{R_{\rm GRB}(z_j)}{(1+z)} \frac{\mathrm{d}V(z)}{\mathrm{d}z} \,. \end{aligned} \tag{4}$$

We also define the *weights factors*

$$w_{ij} \equiv \int_{L_i}^{L_{i+1}} \int_{z_j}^{z_{j+1}} \theta(L,z)\, \mathrm{d}\log L\, \mathrm{d}z \,, \tag{5}$$

as the *probability for detecting a burst with a measured redshift z and luminosity L* where $\theta(L, z) \equiv \theta_z[p(L, z)]$ is the probability to detect and measure redshift for a burst with a luminosity L at a redshift z (see Appendix B). We denote the observed number of events per bin as

$$N_i \equiv N(L_i \le L < L_{i+1}) \,, \tag{6}$$

$$N_{,j} \equiv N(z_j \le z < z_{j+1}) \,, \tag{7}$$

$$N_{ij} \equiv N(L_i \le L < L_{i+1}, z_j \le z < z_{j+1}) \,, \tag{8}$$

$$N \equiv \sum_{ij} N_{ij} \,. \tag{9}$$

Next, we determine ϕ_i and R_j and the error estimates, using the maximum-likelihood formalism. We define M the (logarithmic) likelihood of the model given the observations as

$$M = \sum_{ij} N_{ij} \ln(\phi_i R_j w_{ij}) - N \ln\left(\sum_{ij} \phi_i R_j w_{ij}\right) \,. \tag{10}$$

At the maximum, all partial derivatives of M with respect to ϕ_i and with respect to R_j vanish, leading to

$$\phi_i = \frac{N_i}{\sum_j R_j w_{ij}} \frac{\sum_{i'j'} \phi_{i'} R_{j'} w_{i'j'}}{N} \,, \tag{11}$$

and

$$R_j = \frac{N_{,j}}{\sum_i \phi_i w_{ij}} \frac{\sum_{i'j'} \phi_{i'} R_{j'} w_{i'j'}}{N} \,. \tag{12}$$

Note that the second term on the right-hand side of each of the equations (11) and (12) is the same normalization factor. We have a set of non-linear equations with as many equations as variables. We solve numerically these non-linear equations using successive iterations until convergence. A priori it is not clear whether ϕ and R are uniquely determined and whether there is a solution at all. However, we find good convergence. We have examined a large set (10^8) of initial guesses where each component was randomly drawn from a uniform distribution. We found a rapid convergence to a unique solution for all initial guesses, all reaching the requested accuracy of 10^{-6} with less than 25 iterations. We thus conclude that the existence of other stable solutions is very unlikely.

3.3 Error estimates

We approximate the error as the value for which M deviate by -1 from its maximum (i.e. the likelihood is smaller by a factor e). This reflects an 1σ error for a normal distribution.

$$-1 = N_i \ln\left(1 + \frac{\Delta\phi_i}{\phi_i}\right) - N \ln\left(1 + \frac{N_i}{N}\frac{\Delta\phi_i}{\phi_i}\right) \,, \tag{13}$$

$$-1 = N_{,j} \ln\left(1 + \frac{\Delta R_j}{R_j}\right) - N \ln\left(1 + \frac{N_{,j}}{N}\frac{\Delta R_j}{R_j}\right) \,. \tag{14}$$

The two solutions, i.e. the positive one and the negative one, give an upper and a lower bounds on the error, respectively. For small deviations, we can approximate the error using the second derivatives of M:

$$\frac{\Delta\phi_i}{\phi_i} \simeq \frac{\sqrt{2}}{\sqrt{N_i(1-N_i/N)}} \,, \tag{15}$$

$$\frac{\Delta R_j}{R_j} \simeq \frac{\sqrt{2}}{\sqrt{N_{,j}(1-N_{,j}/N)}} \,. \tag{16}$$

To estimate the uncertainty induced by the specific bins choice, we perform all the analysis for a 1/2 unit redshift and $\mathrm{Log}_{10}(L)$ binning and repeat for a 1/3 unit binning (where all bins widths are 1/3 unit, except the last two redshift bins which we cannot change because they contain too few data points). In the following, unless otherwise stated, we use the 1/2 unit binning for all further analysis. Clearly, the results with different binning are slightly different, but they are all within each other's error range. When we include the uncertainty induced by the binning, the error ranges become only slightly wider.

4 RESULTS

So far, we have not assumed any functional form for the luminosity function or for the rate as our method does not require such an assumption. The 'raw' results are depicted in Figs 2 and 3. Later on we will compare these step functions with models for the GRB rate that follow the SFR. However, in order to easily characterize the result we need to approximate our 'raw' step functions with simple functional forms. Therefore, after obtaining the results in the form of step functions, we approximate them in term of broken power laws:

$$\phi(L) = \begin{cases} \left(\frac{L}{L*}\right)^{-\alpha} & L < L* \,, \\ \left(\frac{L}{L*}\right)^{-\beta} & L > L* \,. \end{cases} \tag{17}$$

$$R_{\rm GRB} = R_{\rm GRB}(0) \begin{cases} (1+z)^{n_1} & z \le z_1 \,, \\ (1+z_1)^{n_1-n_2}(1+z)^{n_2} & z > z_1 \,, \end{cases} \tag{18}$$

We obtain the parameters of the best-fitting functions by minimizing the χ^2 values.

The best-fitting functions are shown (together with the step functions) in Figs 2 and 3. The parameters of the best-fitting models are summarized in Table 1. To estimate the statistical errors involved in the parameter estimates, we preformed a Monte Carlo simulation. In this simulation, we use the model with the best-fitting parameters to draw random sets of data (with same size as the real sample). We then carry out the analysis on this mock data sets and obtain new best-fitting parameters. Repeating this process many

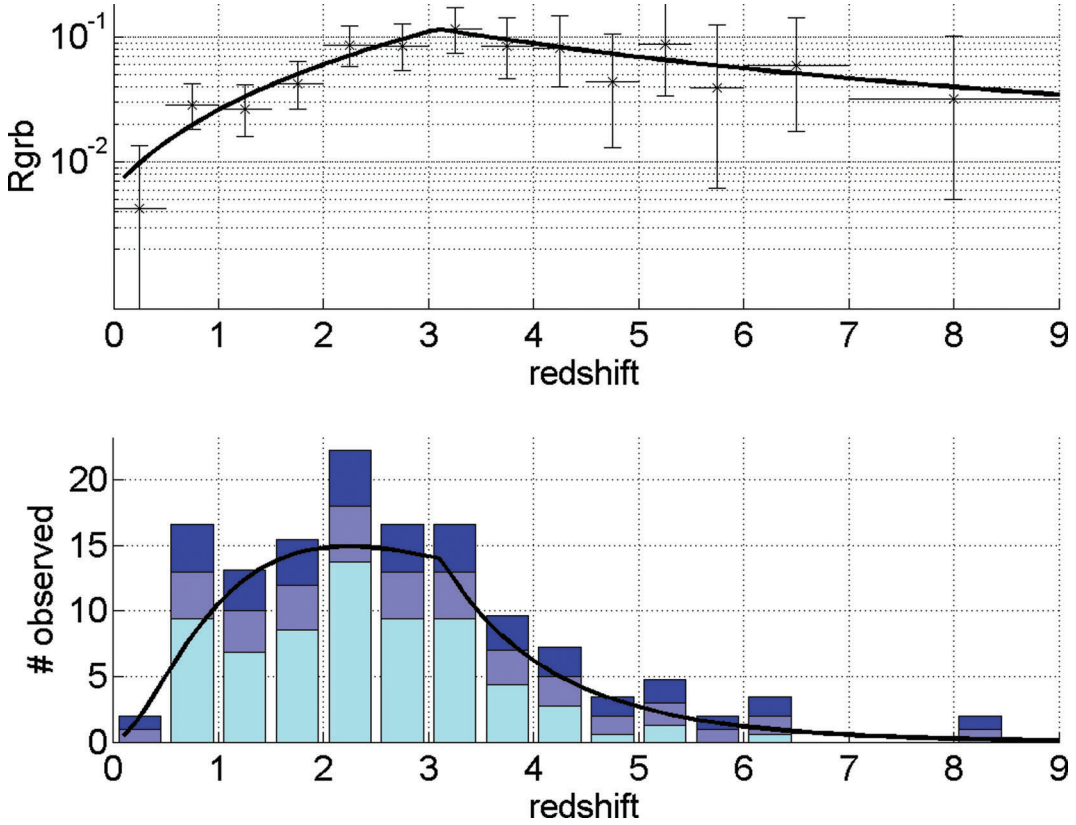

Figure 2. The comoving rate and the observed events number redshift distributions. Upper frame: the resulting step function and the best-fitting model – a broken power law with indices $n_1 = 2.1, n_2 = -1.4$ and with a break at $z = 3.1$ (solid line). The χ^2 values for the models is 2.3 at 10 d.o.f. giving a rejection probability of 0.007. Lower frame: the number of detected bursts for each redshift bin and the rates expected from the model fitted above. The two upper boxes in each column represent the statistical error range.

times we obtain a scatter of points in the parameters plane around the original best-fitting parameters. The central 68 and 95 per cent ranges for each of the parameters separately are also shown in Table 1.

The luminosity function is well described by a broken power law, with a break at $L* \simeq 10^{52.5\pm0.2}$ (erg s^{-1}) and with indices $\alpha = 0.2^{+0.2}_{-0.1}$ and $\beta = 1.4^{+0.3}_{-0.6}$. The broken power-law fit is very good, giving $\chi^2 = 0.63$ for 4 degrees of freedom (d.o.f.). This result agrees with previous studies (e.g. Daigne et al. 2006; Guetta & Piran 2007). The luminosity function cannot be fitted with a single power law, since such fit give high χ^2, rejecting such a model with high significance (98 per cent). This contradicts the results of Pélangeon et al. (2008), who studied the High Energy Transient Explorer (HETE-2) GRBs and found a consistency with a single power-law luminosity function. The rate is described as well by a broken power law for $1 + z$, with a break at $z = 3.1^{+0.6}_{-0.8}$ and indices of $n_1 = 2.1^{+0.5}_{-0.6}$ and $n_2 = -1.4^{+2.4}_{-1.0}$.

The local event rate is $\rho_0 \simeq 1.3^{+0.6}_{-0.7}$ (Gpc^{-3} yr^{-1}), in agreement with previous studies [e.g. Schmidt (1999) ($\rho_0 \simeq 1.5$), see also Schmidt (2001b) ($\rho_0 \simeq 0.15$); Guetta et al. (2005) ($\rho_0 \simeq 0.5$); Guetta & Della Valle (2007) ($\rho_0 \simeq 1.1$); Liang et al. (2007) ($\rho_0 \simeq 1.1$); Pélangeon et al. (2008) ($\rho_0 \gtrsim 0.5$)]. The main factors determining the low-redshift (current) event rate are the overall GRB rate normalization, the low-redshift slope, the low end of the luminosity function slope and most importantly the position of the low-luminosity cut-off. This low-luminosity cut-off is essential for any steep enough power law to prevent its divergence. This cut-off is critical to the question whether the model includes the low-luminosity GRB population. The cut-off used in our estimates of ρ_0 is $L = 10^{50}$ erg s^{-1}.

4.1 Consistency checks

Before we can accept the model, we turn now to check the validity of the assumption that the luminosity function and the rate are independent. To do so, we preform a 2D Kolmogorov–Smirnov (K–S) test (see Peacock 1983; Fasano & Franceschini 1987; Spergel et al. 1987). In this test, the 2D data are compared to the modelled distribution for each of four quadrant defined by axes crossing at each data point. The maximal difference is used to estimate the probability that the data are drawn from the distribution implied by the model. The probability that the models fits the data is displayed in the 2D K–S column in Table 4. The test give high probability (96 per cent), so we can accept the model and justify the underling assumption (of a redshift-independent luminosity function).

We carry out two other consistency checks. First, we compare the peak-flux distribution expected by our model with those observed by BATSE and by *Swift*. The results are shown in Figs 4 and 5. The K-S test results, 83 per cent for BATSE bursts and 17 per cent for the full sample of *Swift* bursts (with or without redshift), indicate acceptable model. We note here that the model is significantly rejected (K–S test $< 10^{-5}$) when compared to BATSE peak-fluxes distribution using $P_{\rm lim} = 0.25$ ph cm^{-2} s^{-1}. However, when applying the effective detection threshold calculated by Band (2002) of

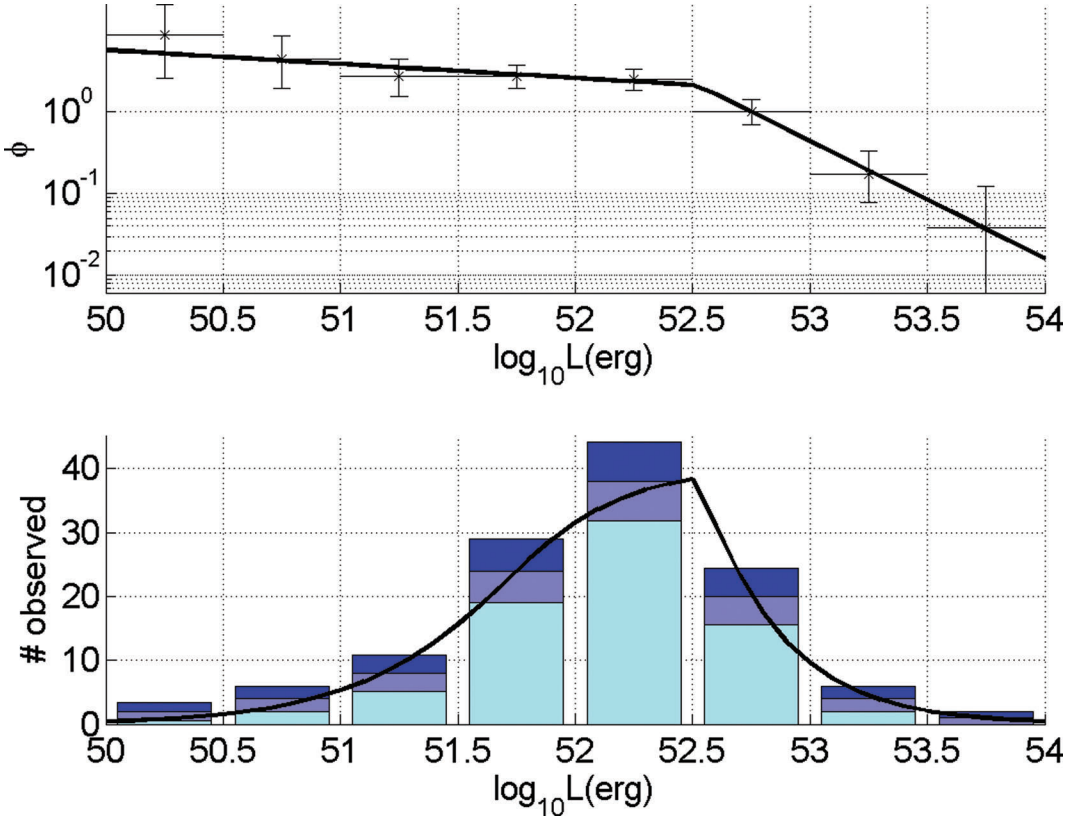

Figure 3. The luminosity function and the observed and predicted luminosity distributions. Upper frame: the resulting step function and the best-fitting model for the luminosity function – a broken power law with a break at $L* = 10^{52.5}$, a low-luminosity index $\alpha = 0.2$ and a high-luminosity index $\beta = 1.4$. The χ^2 value for this model is 0.63 at 4 d.o.f., giving a rejection probability of 0.04. Lower frame: the number of detected bursts for each luminosity bin and the rates expected from the model fitted above. The two upper boxes in each column represent the statistical error range.

Table 1. Parameter results. The error ranges are 68 and 95 per cent levels estimated using a Monte Carlo simulations with 10 000 sets, each of 101 data points.

	1/2 bins	1/3 bins
$\log L*$	$52.53^{+0.24+0.54}_{-0.17-0.66}$	$52.58^{+0.21+0.68}_{-0.14-0.25}$
α	$0.17^{+0.19+0.37}_{-0.10-0.21}$	$0.18^{+0.18+0.37}_{-0.09-0.20}$
β	$1.44^{+0.33+0.59}_{-0.64-7.08}$	$1.59^{+0.36+0.66}_{-0.58-7.86}$
z_1	$3.11^{+0.63+1.35}_{-0.82-1.66}$	$3.45^{+0.95+1.67}_{-0.83-2.64}$
n_1	$2.07^{+0.51+0.89}_{-0.63-1.55}$	$1.74^{+0.41+0.83}_{-0.65-1.61}$
n_2	$-1.36^{+2.39+6.83}_{-1.00-1.41}$	$-1.47^{+2.98+8.53}_{-1.30-1.66}$
ρ_0	$1.25^{+0.56+0.93}_{-0.70-1.52}$	$1.71^{+0.76+1.27}_{-0.74-1.93}$

$P_{\rm lim} = 0.525\,{\rm ph\,cm^{-2}\,s^{-1}}$, the model is accepted with high significance (83 per cent).

Secondly, we compared the cumulative redshift distribution to the observed one and preformed a K–S test. Here, as well, the test gives a high probability for accepting the model (62 per cent).

To illustrate the distribution of bursts, we display the bursts in the *L*–*z* (*Luminosity–Redshift*) plane and in a rescaled plane in which the number of detected bursts (with or without redshift measurement) is proportional to the area (Fig. 6). The rather uniform distribution on the rescaled plane is a visual demonstration of the validity of the assumption.

4.2 A comparison with the complete *Swift* sample

Our results are based only on the absorption and photometric determined redshifts of the *Swift* sample. Recently, Fynbo et al. (2009) obtained emission lines redshift measurements for GRBs host galaxies that were not measured before. Most of those are at low redshifts. The growing number of emission lines redshifts in the range $0 < z < 1$ raises the question whether our model – based on a sample of redshifts measured from the afterglows – is consistent. We calculate, using our model, the expected redshift distribution of the entire bursts population and compare it to the number of observed bursts with a known redshift (measured using all methods). Clearly for any range of redshifts, the number of known bursts with a given redshift range should not exceed the number predicted by the model. Fig. 7 depicts this comparison for the cumulative number and for the counts number in redshift bins. Our model is consistent for all $z \gtrsim 0.4$. However there is an excess of low-redshift bursts not predicted by our model. The discrepancy arises due to three bursts with $z < 0.1$ while less than one burst is predicted by the model. The redshift of the three bursts was determined using emission lines, but no redshift was detected in this range using absorption lines. These three bursts yield a rate that is significantly higher than predicted by the model. This cannot be explained by a mis-identification of the host galaxies because the probability for such an effect is too small

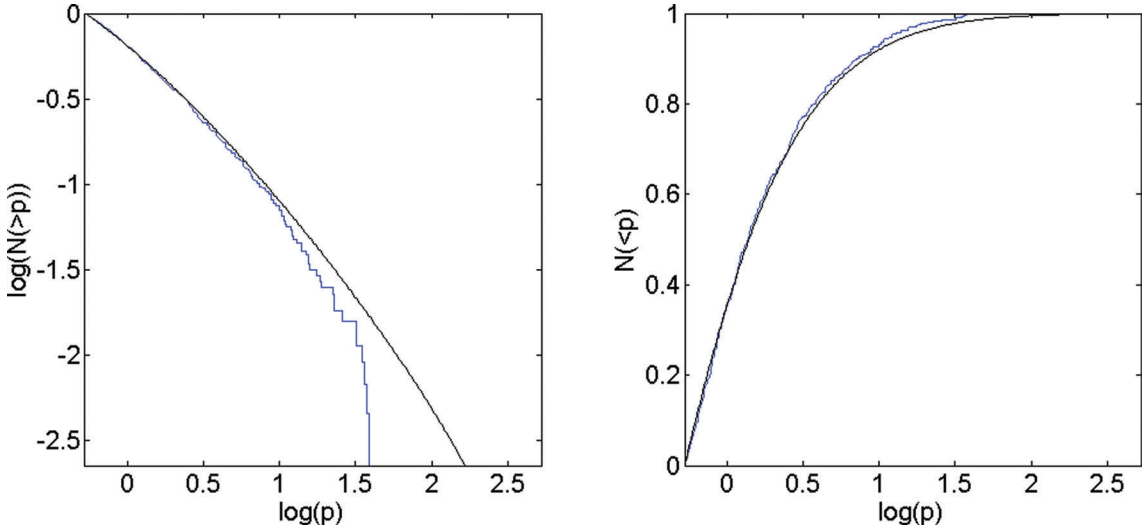

Figure 4. Bursts count versus peak flux for BATSE bursts. Cumulative bursts distribution as a function of the peak flux p. Left: logarithmic scale showing $N(<p)$. Right: log linear scale showing $N(>p)$, this is used for the K–S test, giving probability of 83 per cent.

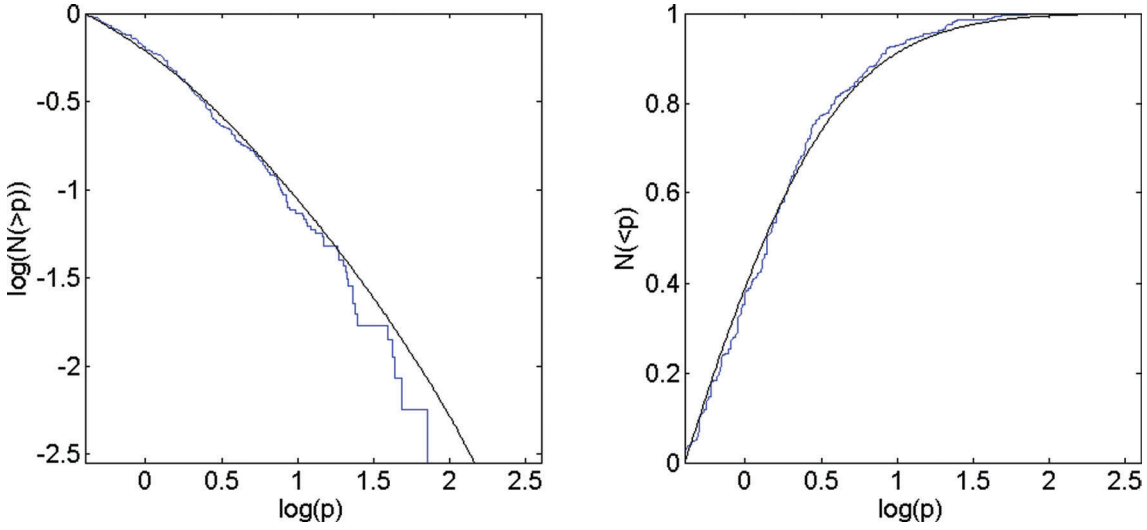

Figure 5. Bursts count versus peak flux for *Swift* bursts. Cumulative bursts number distribution as a function of the peak flux p. Left: logarithmic scale showing $N(<p)$. Right: log linear scale showing $N(>p)$, which is used for the K-S test, giving a probability of 17 per cent.

(Cobb & Bailyn 2008). These low-redshift bursts have low luminosities, and they could not have been detected at a much higher redshift. We conclude that they possibly represent a low-luminosity population that is different from the majority of the bursts (see a discussion in Section 6.2).

4.3 The redshift distribution and expectations for future missions

A particularly interesting question is how many high-redshift bursts are expected to be observed. Such bursts are of great interest as they may shed new light on the very early Universe. Already now GRB 090423 is amongst the most distant and hence the earliest objects observed so far. Fig. 8 depicts the observed cumulative redshift distribution and the predicted one, for high-redshift bursts for *Swift* and for past and future missions: BATSE, EXIST (Band et al. 2008) and SVOM (Schanne 2008; Götz et al. 2009). The fraction of bursts with $z > 7, 8, 9, 10, 15, 20$ respectively is shown in Table 2.

Detection of high-redshift bursts is one of the main objectives of EXIST. The number of high-redshift bursts expected to be detected by EXIST is presented in Table 3. During a 5-yr mission, EXIST will detect many high-redshift ($z > 10$) ($\approx$30) bursts. In the best-fitting model, there is a good probability for EXIST to detect even a $z > 20$ burst during mission. This is, of course, provided that such early bursts exist and that the rate at $z \approx 5$–8 can be extrapolated to such high redshifts.

5 THE GRB RATE AND THE SFR

The location of long GRBs in the star-forming regions led to the expectation that GRB follow the SFR. We turn now to examine this hypothesis. Modelling the SFR throughout the measured redshift range ($0 < z < 10$) is a complicated task, involving observations in various wavelengths and various assumptions on observational proxies for the SFR as well as correcting due to obscuration, absorption and selection effects. In a classical work, Madau (Madau et al.

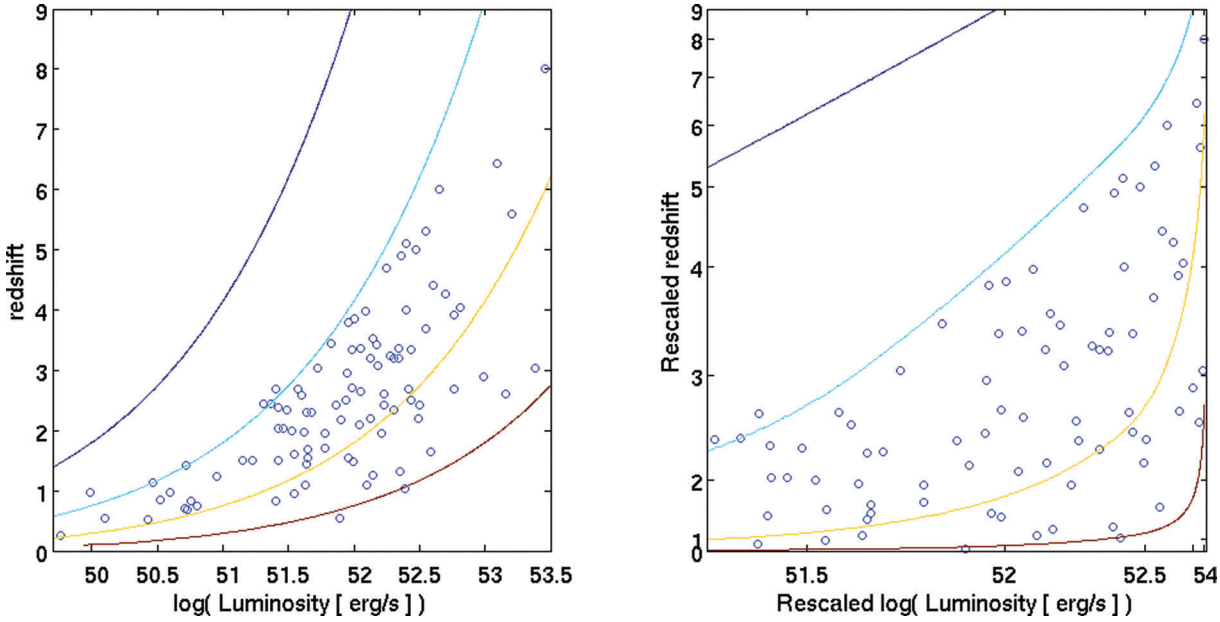

Figure 6. Bursts on the L–z plane. The bursts distribution in the luminosity–redshift plane. Left: linear scale. Right: axes are rescaled using $R(z)$ and $\phi(L)$, so that we have a uniform bursts-number density. The curved lines are contour lines for equal fluxes, for the values, $p = 0.04, 0.4, 4, 40$ (ph s^{-1} cm^{-2}), from top to bottom. The $p = 0.4$ (ph s^{-1} cm^{-2}) line is our detection threshold. The number density is uniform in the rescaled plane as expected and it drops to zero below the detection threshold.

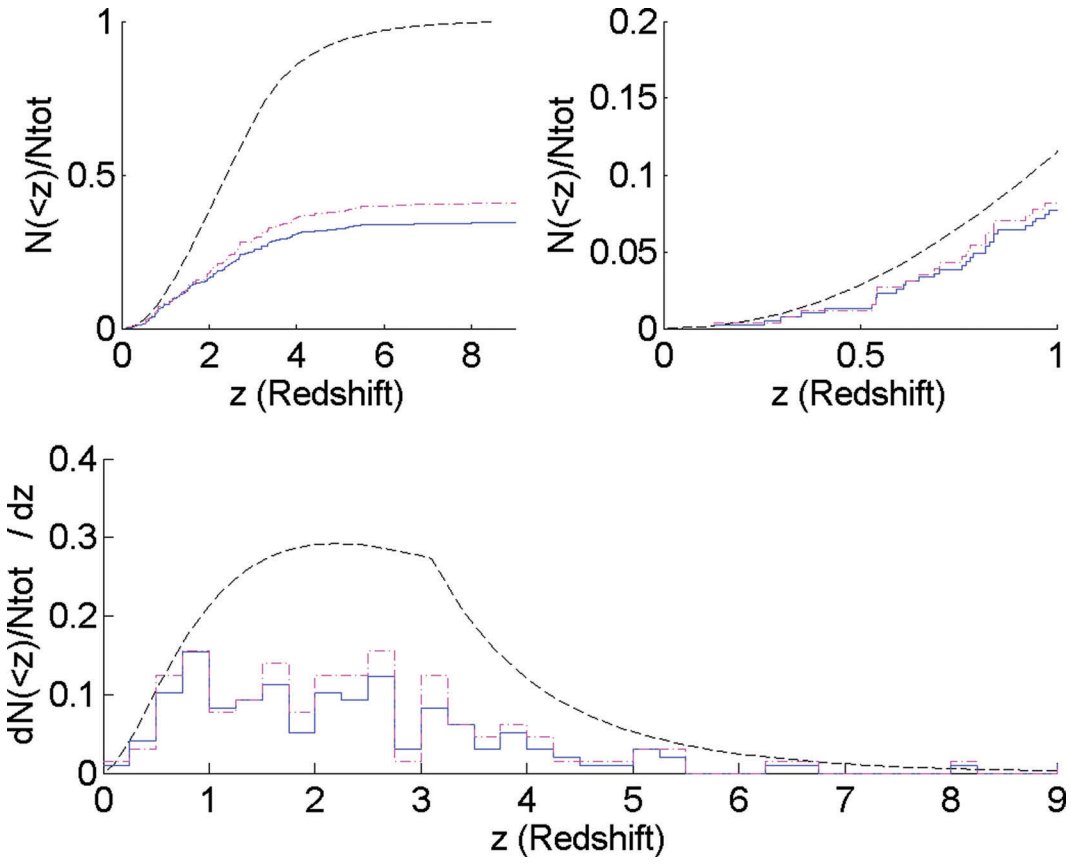

Figure 7. Redshifts obtained by any method compared with the total number of bursts predicted by the model. (Upper frames) Left: the cumulative total fraction of bursts predicted by the model (dashed curve) and the detected cumulative fraction of bursts with redshift obtained by any method (solid steps) as a function of the redshift. Right: zoom-in on the low-redshift part. Lower frame: the number density (per unit redshift) of predicted bursts (dashed curve) and a histogram of bursts with redshift obtained by any method (solid steps). Both are normalized by the total number of bursts. For all frames, the number of bursts with redshifts which had an at slew, i.e. the time elapsed form the trigger until the first optical observation is less than 300 s (dot–dashed steps).

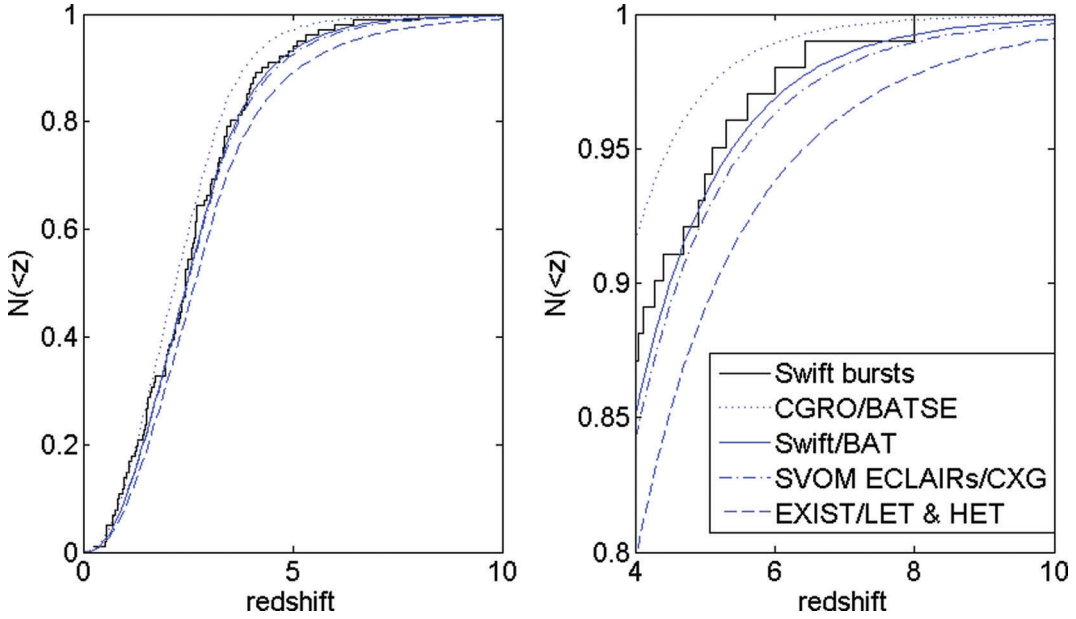

Figure 8. The cumulative redshift distribution for *Swift* bursts and predictions for other missions. The cumulative redshift distribution of *Swift* observed bursts and the model prediction (solid line). The K–S test gives a probability of 62 per cent. Also presented are the predictions for some past and future missions: BATSE, SVOM and EXIST. Right frame is a zoom-in to the upper right part of the left frame.

Table 2. The high-redshift fraction prediction for *Swift* and several other missions.

Fraction of $z >$	7 (per cent)	8 (per cent)	9 (per cent)	10 (per cent)	15 (per cent)	20 (per cent)
CGRO/BATSE	0.4	0.2	0.1	0.05	0.01	0.002
Swift/BAT	1.7	0.9	0.5	0.3	0.03	0.01
SVOM ECLAIRs/CXG	2	1.2	0.7	0.4	0.06	0.02
EXIST/LET & HET	4	3	2	1	0.2	0.06

Table 3. High-redshift detection rates prediction for EXIST and for SVOM. On average a redshift is obtained for only a third of the events.

Bursts per year for $z >$	7	8	9	10	15	20
EXIST	23^{+121}_{-12}	14^{+96}_{-8}	9^{+81}_{-6}	6^{+64}_{-4}	$0.9^{+25.1}_{-0.7}$	$0.2^{+11.8}_{-0.16}$
SVOM	2^{+12}_{-1}	$1^{+9}_{-0.5}$	$0.7^{+6.3}_{-0.5}$	$0.4^{+4.6}_{-0.3}$	$0.06^{+1.94}_{-0.05}$	$0.01^{+0.79}_{-0.007}$

1996; Madau 1997; Madau, Pozzetti & Dickinson 1998) considered the SFR per comoving volume versus redshift and found a rise from present to $z \approx 1$–2, and then a comparable decline to $z \approx 5$. This form of the SFR versus redshift has become known as the 'Madau plot'. A number of developments (e.g. dust corrections, submm results, new estimates of the SFR at low redshift) led to changes in the shape of the SFR. Following these developments Rowan-Robinson (1999) and Porciani & Madau (2001) suggested that the SFR rises by a factor of 10–20 from $z = 0$ to $z \simeq 1$. The rate at higher redshifts ($z > 2$) was undecided at that time and models for the SFR at higher redshift included flat as well as rising and declining functions (Porciani & Madau 2001). Later, Hopkins & Beacom (2006) showed that at high redshift ($z > 4$), the SFR declines. Recently, several papers estimated the SFR using the new *Hubble Space Telescope* WFC3/IR camera (Bouwens et al. 2009a,b; Yan et al. 2009; Bunker et al. 2010; McLure et al. 2010; Oesch et al. 2010). These works suggest a decline in the SFR for $z \gtrsim 4$ up to $z \sim 8$–9 . In the following, we use Bouwens et al. (2009b) as representative of these new high-z SFRs. Despite all the observational advances, there are still different models of the SFR even at low ($z < 1$) and intermediate ($1 < z < 3$) redshift. On one hand, the widely used Hopkins & Beacom (2006) piecewise linear fit finds a factor 10 rise in the SFR from $z = 0$ to 1 and an almost constant rate from $z = 1$ to 4.5 (which follows by a steep decline at higher redshifts). On the other hand, Bouwens et al. (2009b) use data from Schiminovich et al. (2005) and Reddy & Steidel (2009) for $0 < z < 2, 2 < z < 3$, respectively. Their data compilation can be fairly modelled ($\chi^2 = 10.8$ for 9 d.o.f.) by a broken power law rising a factor of 20 from $z = 0$ to 3.3, then declining as $(1 + z)^{-5.8}$ for $3.3 < z$. Note that a rise up to $z =$ 2–3 is also suggested by Hopkins & Beacom (2006) when fitting to a Cole (2001) form. This seemingly mild disagreement between different SFR models have a crucial implication when comparing the GRB rate to the SFR.

The same tests used in Section 4.1 can be used now to check the consistency of the data with a rate proportional to the SFR. An obvious problem is that SFR is not uniquely determined and hence

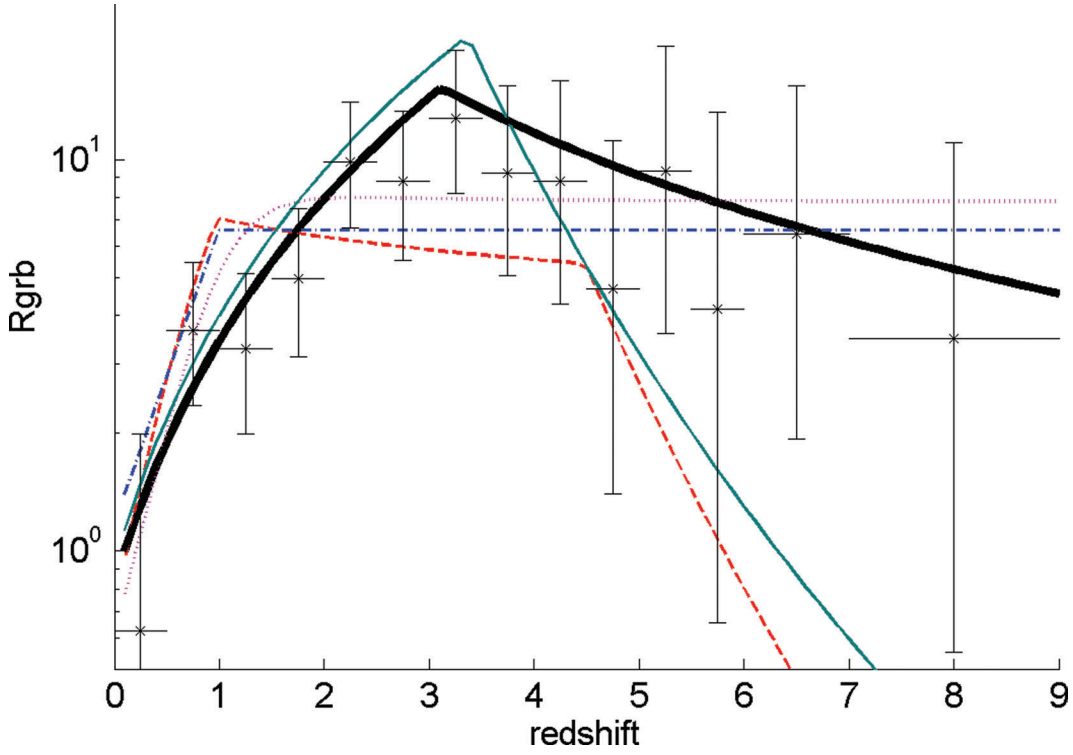

Figure 9. GRB event rate and several SFRs. The results for the rate, in 1/2 unit binning. Best fit for a broken power law – heavy black solid line. Hopkins & Beacom (2006) SFR – dashed line, Bouwens et al. (2009b) SFR – solid line. SF2 of Porciani & Madau (2001) – dotted line. Rowan-Robinson (1999) SFR – dashed dotted line.

we consider four different possible functions: Hopkins & Beacom (2006) (denoted HB), SF2 of Porciani & Madau (2001) (denoted PM SF2), Rowan-Robinson (1999) (denoted R-R) and Bouwens et al. (2009b) (denoted B09). Note that HB and B09 decrease at large redshift, while PM SF2 and R-R stay constant. We compare, first, the SFRs to the binned rate we obtained by inverting the data (see Fig. 9), and we calculate the χ^2 for both 1/3 and 1/2 binning. We find acceptable reduced χ^2 values (see Table 4) for all the functions. However, a comparison of the overall observed redshift and luminosity distributions with those predicted by models in which the GRB rate is fixed by a given SFR reveals that the 2D K–S or the K–S tests for the peak flux and the redshift distributions show inconsistency for the first three functions (HB, PM SF2, R-R). We find, however, consistency for the last one (B09).

Next, we optimize the luminosity function for a given SFR. We take the GRB rate as known following a model of the SFR and obtain the best-fitting luminosity function by solving equation (12). We now perform a 2D K–S test as well as K–S tests for the peak-flux distribution and for the redshift distribution. The results of the statistical tests are shown in Table 4. Even though the fit improves, still the first three SFR models fail the K–S tests. The last SFR model (B09) is, of course, consistent.

Table 4. Statistical tests for our models and for models following one of the SFRs considered (upper part) and for GRB rate from other studies (lower part). The consistent models are marked with a bold font. For each model, we show the test with luminosity function from our results (first line) and with luminosity function that best-fitting observations after forcing the rate to follow the SFR (second line).

	Reduced χ^2 (1/3 bins)	Reduced χ^2 (1/2 bins)	2D K–S	Peak flux K–S test	z K–S test	$L*$	α	β	ρ_0
This paper	0.24	0.23	0.96	0.82	0.62	52.53	0.17	1.44	1.25
R-R(1999)	0.69	0.85	2×10^{-3}	1×10^{-3}	9×10^{-5}	52.53	0.19	1.44	2.04
R-R(1999)			0.05	2×10^{-5}	0.01	52.46	−0.06	1.48	1.40
HB	1.14	1.38	1×10^{-5}	1×10^{-4}	4×10^{-8}	52.53	0.19	1.44	1.30
HB			2×10^{-3}	6×10^{-9}	6×10^{-5}	52.49	−0.12	1.46	0.83
PM SF2	0.53	0.58	0.05	0.05	0.01	52.53	0.19	1.44	1.01
PM SF2			0.17	0.01	0.07	52.47	−0.00	1.48	0.75
B09	**0.57**	**0.60**	**0.21**	**0.93**	**0.14**	**52.53**	**0.19**	**1.44**	**1.22**
B09			**0.15**	**0.65**	**0.19**	**52.53**	**0.08**	**1.47**	**0.99**
Butler et al. (2009)	**0.27**	**0.27**	**0.76**	**0.65**	**0.71**	**52.53**	**0.19**	**1.44**	**0.80**
Butler et al. (2009)			**0.66**	**0.46**	**0.50**	**52.47**	**0.00**	**1.47**	**0.58**

We attribute the consistency of the GRB rate with the B09 SFR model but not with the first three SFR models to the difference between the B09 SFR and the other three models in the range $1 < z < 3$. While B09 keeps increasing in this range the first three are constant. This difference is crucial, and understanding the SFR at this region is critical for the question whether the GRB rate follows the SFR or not. While there are differences at higher redshifts, the paucity of data leads to wide error range in that region allowing the GRB observations to be consistent with SFRs that are constant, decreasing or even increasing at large z.

The comparison table shows that the luminosity function parameters depend very weakly on the GRB rate model. α and ρ_0 changes within their 95 per cent error range, while $L*$ and β stay almost unchanged. This illustrates the power of the method and the robustness of the luminosity function results, in particular for $L*$ and β.

5.1 Comparison with other works

Our results are in agreement with most previous works on the GRB rate. Our results agree with Daigne et al. (2006), who compared the *Swift* data with Porciani & Madau (2001) SFR models and concluded that the rising model SF3 is the only one consistent (our model is also consistent with SF3). We stress, however, that the recent work on the SFR suggests that it decreases at high redshift and thus SF3 is, most likely, not a viable SFR model. Our results are also consistent with Guetta & Piran (2007), who find that at $z > 2.5$ the GRB rate is significantly higher than the R-R or PM SF2 SFR.

A comprehensive work studying the luminosity function and the rate of long GRBs was recently published (Butler, Bloom & Poznanski 2009). While this work uses a different sample, adopts somewhat different assumptions and uses other methods, a comparison of the results can be very useful. We find a good agreement for the low-luminosity power-law index $\alpha = 0.22^{+0.18}_{-0.31}$ (our results : $0.2^{+0.2}_{-0.1}$) and for the break luminosity $L* = 10^{52.74\pm0.43}$ (our results : $10^{52.5\pm0.2}$). However, we find different high-luminosity power-law index $\beta = 2.9^{+2.1}_{-1.1}$ (our results: $1.4^{+0.3}_{-0.6}$). The differences may be explained by the fact that Butler et al. (2009) use a luminosity which is a time-averaged, whereas our luminosity is the peak luminosity. We find a nice agreement between the models for the GRB rate. Butler et al. (2009) find a rising rate for $0 < z < 4$: first, at slope 3.1 ± 0.7 for $0 < z < 1$ and later at slope 1.4 ± 0.6 for $1 < z < 4$. This is not very different from our results, recalling that the break at $z = 1$ was not a free parameter in their model. The decline slope for $z > 4$ is $-2.9^{+1.6}_{-2.4}$, but with the big uncertainties it also matches our model. It is thus not surprising that their model shows consistency with the statistical tests (see Table 4). Another useful comparison is with Kistler et al. (2009), who modelled the bias of the GRB rate with SFR in the range $0 < z < 4$ and used it together with the high-z bursts data to estimate the high-z SFR. The high-z GRB rate they found is roughly constant, in agreement with our results.

6 SUMMARY AND CONCLUSIONS

We find that the GRB rate increases up to $z \simeq 3$ and it decreases at $z > 3$ ($n_2 \simeq -1.4$), with 68 per cent confidence limits ranging from a steep decline ($n_2 \simeq -2.4$) to a positive incline ($n_2 \simeq 1$). The rate is compatible, of course, with a constant rate at higher redshifts. The model is consistent with all statistical tests, and thus we can accept the basic assumption that the luminosity function dose not evolve with time.

6.1 GRB rate and the SFR

The comparison between the SFR and the GRB rate seems to be inconclusive. This arises because of the differences between different estimates of the SFR at the intermediate redshift range $1 < z < 3$. The rate we find is consistent with B09 (that follows Schiminovich et al. 2005) that describes a rising SFR from present up to $z \approx 3$. It is inconsistent with other SFRs (Rowan-Robinson 1999; Porciani & Madau 2001; Hopkins & Beacom 2006) that suggest a constant rate at this regime.

At high redshifts the GRB data are sparse. The best-fitting result decreases slower than the most recent B09 SFR (or even the HB SFR) suggesting possibly higher GRB rate. However fast decrease, like B09, cannot be ruled out while a flat or even slowly increasing rate is also consistent. A larger GRB rate at high redshift (compared to the SFR) can be explained within the framework of the massive stellar collapse model due to metallicity. Woosley & Heger (2006) suggests that GRB rate follows the low-metallicity part of the star formation. We cautiously note however that Fynbo et al. (2009) recently found that the optical afterglow spectroscopy sample is biased against measuring redshift at high-metallicity environments, meaning that the result might be an artefact of a selection effect. Another clue can be taken from Fruchter et al. (2006) who found that the GRBs distribution within the host galaxies does not follow the light distribution but rather some power (>1) of the light distribution, i.e. higher GRB density in the denser star-forming regions. This is in contrast to the core-collapse supernovae distribution that follows the light distribution, indicating the GRB progenitors are different from supernova progenitors and hence their rate might be different.

6.2 Low-luminosity bursts

We find an overall consistency when comparing our model and the full sample of GRBs with redshift. However, we also find three low-redshift, low-luminosity bursts (with emission lines redshifts) that are not expected by the model prediction. The faintest burst in our sample GRB 050724 has a luminosity $L_1 = 10^{50.4}$ (erg s^{-1}). By applying our best-fitting model, we expect 0.9 bursts with luminosity $L \leq L_1$, in the time-span of our sample (4.5 yr). *Swift*'s weakest burst, GRB 060218 (Cusumano et al. 2006) with luminosity $L_2 = 10^{47.4}$ (erg s^{-1}), is not in our sample because it has only emission lines redshift. Assuming that we can extrapolate the low end of our luminosity function, we expect 2.5×10^{-6} bursts with $L \leq L_2$. Even when applying the 95 per cent level of the parameter $\alpha = 0.38$, we expect no more than 5×10^{-5} bursts with $L \leq L_2$. This implies that this burst represents a population of fainter GRBs, with much higher event rate, which cannot be directly extrapolated from the stronger GRB population (in agreement with e.g. Cobb et al. 2006; Soderberg et al. 2006; Guetta & Della Valle 2007; Liang et al. 2007). The emission lines redshifts sample includes two other low-luminosity bursts: GRB 051109 and GRB 060505 with $z = 0.08$, 0.089 and $L = 10^{48.6}$ (erg s^{-1}), $10^{49.4}$ (erg s^{-1}). The detection probability of such bursts, according to our model is $<2 \times 10^{-3}$, $<2 \times 10^{-2}$ respectively. These three low-luminosity bursts must belong to a different and a distinct group, and we remove them from the analysis when checking for consistency in Section 4.2.

6.3 High-redshift bursts

Higher redshift bursts are most interesting as they can provide clues on the very early Universe. Extrapolating the rate for very high

redshifts, we expect ∼0.9 bursts with $z > 8$ and ∼0.5 bursts with $z > 9$ (bursts with measured redshift), detected by *Swift* in the time-span of our sample (4.5 yr). This is consistent with the observation of one $z > 8$ burst. Future missions like EXIST can find many more such bursts, even dozens of $z > 10$ bursts (see Section 4.3) provided that a simple extrapolation indeed holds to such high redshifts.

6.4 The local event rate

The local event rate found is $\rho_0 = 1.3^{+0.6}_{-0.7}$ (Gpc^{-3} yr^{-1}), for bursts with $L \geq 10^{50}$ erg s^{-1}. With one galaxy in 100 Mpc^3, this rate is equivalent to 1 event per galaxy per 10^7 yr! Taking into consideration the beaming factor of about 50 (see Guetta et al. 2005), the total events rate is about 1 event per galaxy per 2×10^5 yr. This should be typical to our Galaxy as a recent estimation to the SFR in our Galaxy (Robitaille & Whitney 2010) finds $\dot{\rho} = 0.68$–1.45 M$_\odot$ yr^{-1}, which is equivalent to the SFR in the local Universe for a galaxy in a volume of 100 Mpc^3. One implication of this result will be on the possible association of GRBs with global extinctions of biological species. These occurred on Earth a factor of 10 times less frequently, about once every 100 Myr. These two rates suggest that a typical Galactic GRB pointing to Earth does not cause a major extinction event.

ACKNOWLEDGMENTS

We thank Shiho Kobayashi, Ehud Nakar and Elena Rossi for fruitful discussions, and Nat Butler, John Beacom, Jean-Luc Atteia and Ruben Salvaterra for helpful comments. The research was supported by an ERC Advanced Research Grant, by the ISF center for High Energy Astrophysics and by the Israel–France program in Astrophysics grant.

REFERENCES

Band D. L., 2002, ApJ, 578, 806
Band D. L., 2006, ApJ, 644, 378
Band D. L. et al., 1993, ApJ, 413, 281
Band D. L. et al., 2008, ApJ, 673, 1232
Barthelmy S. et al., 2005, Space Sci. Rev., 120, 143
Berger E. et al., 2005, ApJ, 634, 501
Bouwens R. J., et al., 2009a, ApJ, 705, 936
Bouwens R. J., et al., 2009b, Nat, submitted (arXiv:0912.4263v2)
Bromm V., Loeb A., 2006, ApJ, 642, 382
Bunker A. et al., 2010, MNRAS, submitted (arXiv:0909.2255)
Butler N. R., Bloom J. S., Poznanski D., 2009, ApJ, 711, 495
Chary R., Berger E., Cowie L., 2007, ApJ, 671, 272
Cobb B. E., Bailyn C. D., 2008, ApJ, 677, 1157
Cobb B. E., Bailyn C. D., van Dokkum P. G., Natarajan P., 2006, ApJ, 645, L113
Cohen E., Piran T., 1995, ApJ, 444, L25
Cole S. et al., 2001, MNRAS, 326, 255
Coward D. M., 2008, MNRAS, 393, L65
Cusumano G., Barthelmy S., Gehrels N., Hunsberger S., Immler S., Marshall F., Palmer D., Sakamoto T., 2006, GRB Coordinates Network, 4775
Daigne F., Rossi E. M., Mochkovitch R., 2006, MNRAS, 372, 1034
Fasano G., Franceschini A., 1987, MNRAS, 225, 155
Fenimore E. E. et al., 1993, Nat, 366, 40
Fiore F., Guetta D., Piranomonte S., D'Elia V., Antonelli L. A., 2007, A&A, 470, 515
Firmani C., Avila-Reese V., Ghisellini G., Tutukov A. V., 2004, ApJ, 611, 1033
Firmani C., Avila-Reese V., Ghisellini G., Tutukov A. V., 2005, Nuovo Cimento C, 28, 665
Fruchter A. S. et al., 2006, Nat, 441, 463
Fynbo J. P. U. et al., 2009, ApJS, 185, 526
Galama T. J. et al., 1998, Nat, 395, 670
Gorosabel J., Lund N., Brandt S., Westergaard N. J., Castro Cerón J. M., 2004, A&A, 427, 87
Götz D. et al., 2009, in Meegan C., Kouveliotou C., Gehrels N., eds, AIP Conf. Proc. Vol. 1133, Gamma-Ray Burst: Sixth Huntsville Symposium. Am. Inst. Phys., New York, p. 25
Guetta D., Della Valle M., 2007, ApJ, 657, L73
Guetta D., Piran T., 2005, A&A, 435, 421
Guetta D., Piran T., 2007, J. Cosmol. Astropart. Phys., 7, 3
Guetta D., Piran T., Waxman E., 2005, ApJ, 619, 412
Hopkins A. M., Beacom J. F., 2006, ApJ, 651, 142
Jakobsson P. et al., 2006, A&A, 447, 897
Kistler M. D., Yüksel H., Beacom J. F., Hopkins A. M., Wyithe J. S. B., 2009, ApJ, 705, L104
Kocevski D., Liang E., 2006, ApJ, 642, 371
Le T., Dermer C. D., 2007, ApJ, 661, 394
Le Floc'h E., Charmandaris V., Forrest W. J., Mirabel I. F., Armus L., Devost D., 2006, ApJ, 642, 636
Liang E., Zhang B., Virgili F., Dai Z. G., 2007, ApJ, 662, 1111
Lloyd-Ronning N. M., Fryer C. L., Ramirez-Ruiz E., 2002, ApJ, 574, 554
Loredo T. J., Wasserman I. M., 1998, ApJ, 502, 75
McLure R. J., Dunlop J. S., Cirasuolo M., Koekemoer A. M., Sabbi E., Stark D. P., Targett T. A., Ellis R. S., 2010, MNRAS, 403, 960
Madau P., Ferguson H. C., Dickinson M. E., Giavalisco M., Steidel C. C., Fruchter A., 1996, MNRAS, 283, 1388
Madau P., 1997, in Holt S. S., Olin F. W., Mundy L. G., eds, AIP Conf. Proc. Vol. 393, Star Formation, Near and Far. Am. Inst. Phys., New York, p. 481
Madau P., Pozzetti L., Dickinson M., 1998, ApJ, 498, 106
Mao S., Paczynski B., 1992, ApJ, 388, L45
Matsubayashi T., Yamazaki R., Yonetoku D., Murakami T., Ebisuzaki T., 2005, Prog. Theor. Phys., 114, 983
Natarajan P., Albanna B., Hjorth J., Ramirez-Ruiz E., Tanvir N., Wijers R., 2005, MNRAS, 364, L8
Oesch P. A. et al., 2010, ApJ, 709, L16
Paczyński B., 1998, ApJ, 494, L45
Peacock J. A., 1983, MNRAS, 202, 615
Pélangeon A. et al., 2008, A&A, 491, 157
Piran T., 1992, ApJ, 389, L45
Porciani C., Madau P., 2001, ApJ, 548, 522
Preece R. D., Briggs M. S., Mallozzi R. S., Pendleton G. N., Paciesas W. S., Band D. L., 2000, ApJS, 126, 19
Reddy N. A., Steidel C. C., 2009, ApJ, 692, 778
Robitaille T. P., Whitney B. A., 2010, ApJ, 710, L11
Rowan-Robinson M., 1999, Ap&SS, 266, 291
Salvaterra R., Chincarini G., 2007, ApJ, 656, L49
Salvaterra R., Guidorzi C., Campana S., Chincarini G., Tagliaferri G., 2009, MNRAS, 396, 299
Schanne S., 2008, in Galassi M., Palmer D., Fenimore E., eds, AIP Conf. Proc. Vol. 1000, Gamma-Ray Bursts 2007. Am. Inst. Phys., New York, p. 581
Schiminovich D. et al., 2005, ApJ, 619, L47
Schmidt M., 1999, ApJ, 523, L117
Schmidt M., 2001a, ApJ, 552, 36
Schmidt M., 2001b, ApJ, 559, L79
Soderberg A. M. et al., 2006, Nat, 442, 1014
Spergel D. N., Piran T., Loeb A., Goodman J., Bahcall J. N., 1987, Sci, 237, 1471
Totani T., 1997, ApJ, 486, L71
Totani T., 1999, ApJ, 511, 41
Ulmer A., Wijers R. A. M. J., 1995, ApJ, 439, 303
Ulmer A., Wijers R. A. M. J., Fenimore E. E., 1995, ApJ, 440, L9
Wijers R. A. M. J., Bloom J. S., Bagla J. S., Natarajan P., 1998, MNRAS, 294, L13
Woosley S. E., Heger A., 2006, ApJ, 637, 914

Yan H., Windhorst R., Hathi N., Cohen S., Ryan R., O'Connell R., McCarthy P., 2009, ApJ, submitted (arXiv:0910.0077v2)
Yüksel H., Kistler M. D., 2007, Phys. Rev. D, 75, 083004
Yüksel H., Kistler M. D., Beacom J. F., Hopkins A. M., 2008, ApJ, 683, L5

APPENDIX A: THE LUMINOSITY

In this work we used only data collected by *Swift*. The peak flux of each burst, measured in *Swift*'s Burst Alert Telescope (BAT) detectors band 15–150 keV (Barthelmy et al. 2005). For most of the bursts, we cannot estimate the luminosity in the full γ-range (1 keV–10 MeV) as the spectral shape (the Band-function) (Band et al. 1993) is poorly known. We still need however to have some quantitative measure of the luminosity that will be defined uniformly for all burst with a known redshift. To do so we use an average characteristic Band function, $E_{\rm peak} = 511$ keV (in source frame), $\alpha = -1, \beta = -2.25$ (Preece et al. 2000; Porciani & Madau 2001) to estimate luminosity, using the same parameters for all bursts, thus the estimated luminosity is proportional to the measured *peak flux* (p):

$$L_{\rm iso} = p 4\pi D(z)^2 (1+z) k(z) C_{\rm det}\ , \tag{A1}$$

$D(z)$ is the proper distance at redshift z, $C_{\rm det}^{-1}$ is the fraction of the total gamma-ray luminosity detected in the detectors energy band for source at $z = 0$,

$$C_{\rm det} = \frac{\int_{1\,{\rm keV}}^{10\,{\rm MeV}} E N(E){\rm d}E}{\int_{E_{\rm min}}^{E_{\rm max}} N(E){\rm d}E}\ , \tag{A2}$$

$k(z)$ is the k-correction for the given spectrum at redshift z,

$$k(z) = \frac{\int_{E_{\rm min}}^{E_{\rm max}} N(E){\rm d}E}{\int_{(1+z)E_{\rm min}}^{(1+z)E_{\rm max}} N(E){\rm d}E}\ , \tag{A3}$$

where $N(E)$ is the Band function, $E_{\rm min} = 15$ keV, $E_{\rm min} = 150$ keV. The values in this paper are the luminosity in the range (1 keV – 10 MeV).

To study the dependence of our results on this approximation of an average Band function, we have preformed a simulation where the spectrum of the bursts is not universal but drawn randomly from the known distribution (Preece et al. 2000). Repeating the analysis in the paper 1000 times, each time calculating the luminosity of a burst using a Band function with parameters randomly drawn – independently for each burst – from the distribution. Fig. A1 show the simulation results as a histogram for each of the parameters of the luminosity function and the rate fits. All the distributions concentrate within the 68 per cent error range of the original results, demonstrating the robustness of the results and its insensitivity to the details of the distribution of spectral parameters.

APPENDIX B: THE REDSHIFT DETECTION PROBABILITY

We examine now the redshift detection probability as a function of the *peak flux*. We consider here two effects: first, the probability to detect the GRB and second the probability to measure the redshift, for a given detected burst.

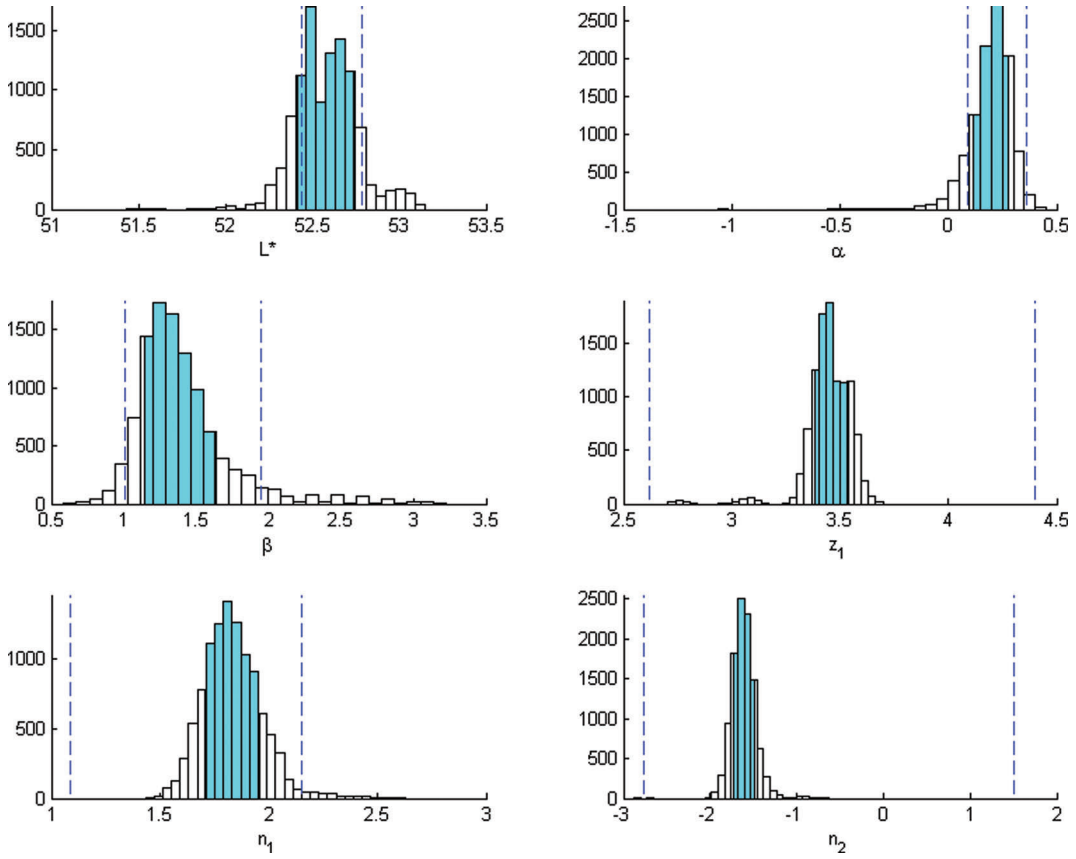

Figure A1. Distributions of our fits parameters for the luminosity function ($L*$, α, β) and for the rate (z_1, n_1, n_2) when choosing the gamma-ray spectra (Band function) parameters randomly from their distributions. The shaded area contains the central 68 per cent of the distribution, the dashed lines are the 68 per cent confidence range of our reported results.

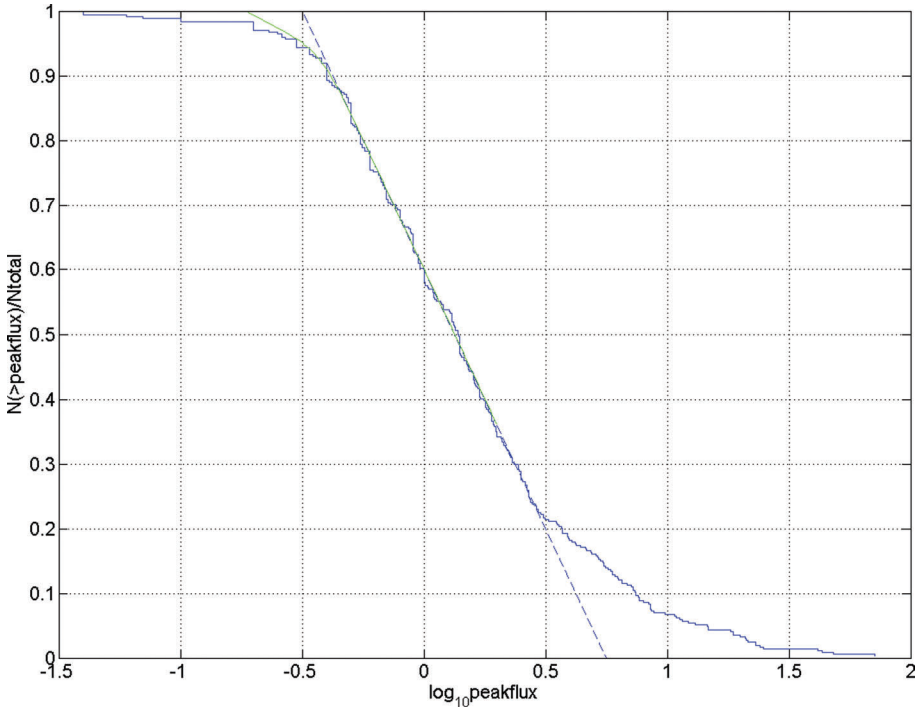

Figure B1. The accumulated number of bursts as function of log(peak flux).

The probabilities to detect a GRB, or to measure a redshift, are a function of the burst energy, its duration and other factors, as described by Band (2006). We restrict ourselves here only to the dependence of these probabilities in the *peak flux*, since this is the quantity we use for the analysis in this paper.

B1 GRB detection probability

The simplest model often used is of a sharp threshold: no detection with $p < p_{\rm lim}$, but 100 per cent detection of bursts with $p \geq p_{\rm lim}$. For this model, the value used at *Swift*'s main detection band (15–150) keV is $p_{\rm lim} = 0.4\,{\rm ph\,cm^{-2}\,s^{-1}}$ (see Guetta & Piran 2007;

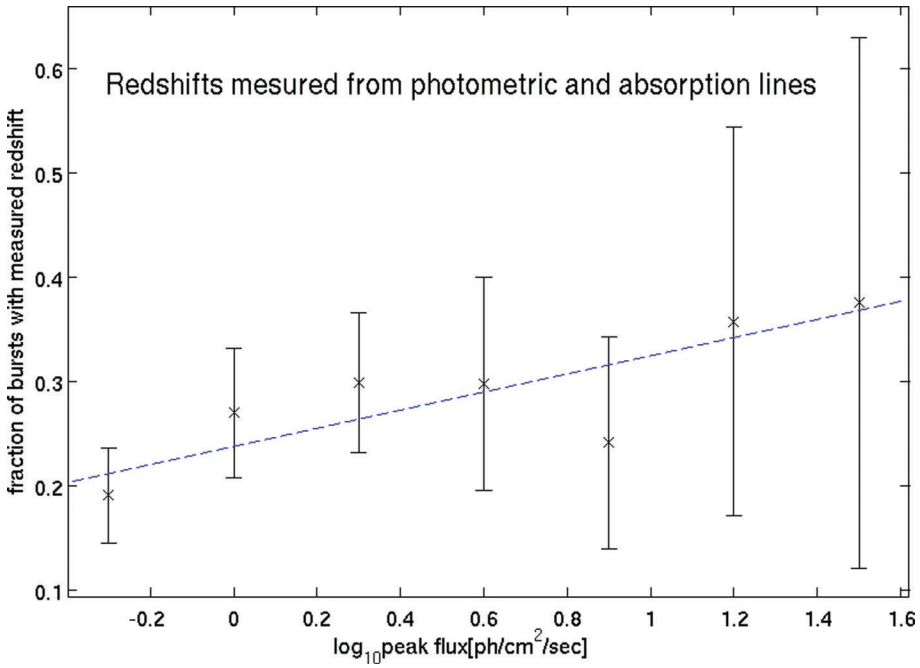

Figure B2. The fraction of bursts with a measured absorption lines and photometry redshift, as function of log(p).

Gorosabel et al. 2004). In the plot of the accumulated number of bursts as a function of $\log(p)$, a linear relation appears for fluxes that are low or medium but above the threshold mentioned above. Although we do not try to give a theoretical explanation for this result, we do not expect however any strong deviation from that connection for lower fluxes, since our models predict a slow gradual smooth change in $\mathrm{d}N/\mathrm{d}\log(p)$ and we can adopt this values at least as an order of magnitude estimators, to yield a continuous threshold estimation. Assuming that the deviation from linearity for fluxes below $p_{\rm lim}$ is only due to a lowered detection sensitivity; we can extrapolate the predicted number of bursts for lower fluxes and extract the detection sensitivity by comparing the number of detected bursts to the predicted number. Fig. B1 shows this: accumulated number of bursts versus $\log(p)$, the linear fit and our fit.

$$\theta_\gamma(p) = \begin{cases} \frac{(1+c)}{2} + \frac{(1-c)}{2}\mathrm{erf}(d\log(p/p_0)) & p \geq 0.2, \\ 0 & p < 0.2, \end{cases} \quad \text{(B1)}$$

with the parameters found:

$c = 0.25, \quad d = 10, \quad \log_{10} p_0 = -0.42.$

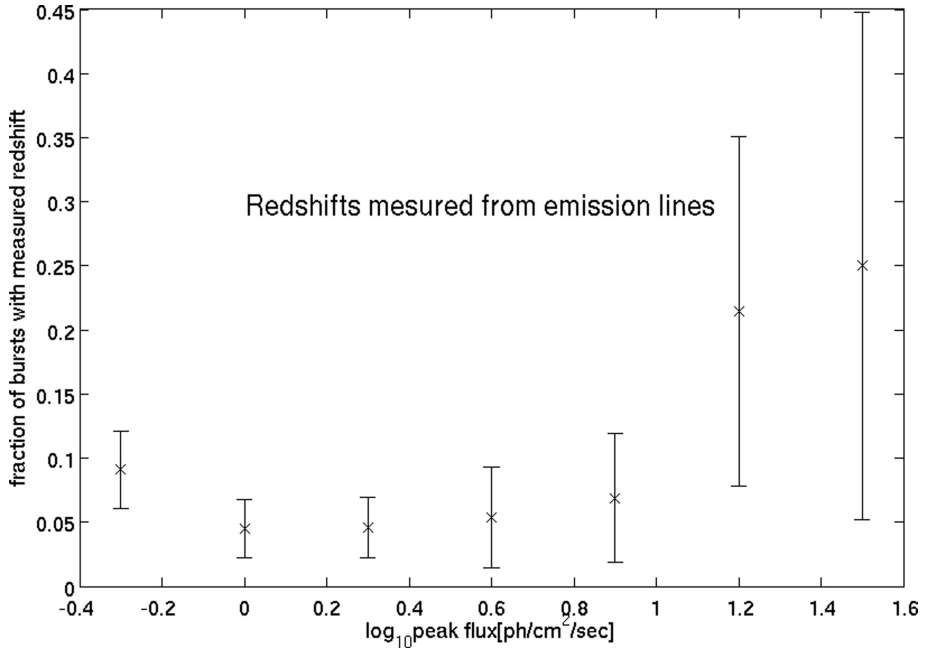

Figure B3. The fraction of bursts with a measured emission line redshift, as function of $\log(p)$.

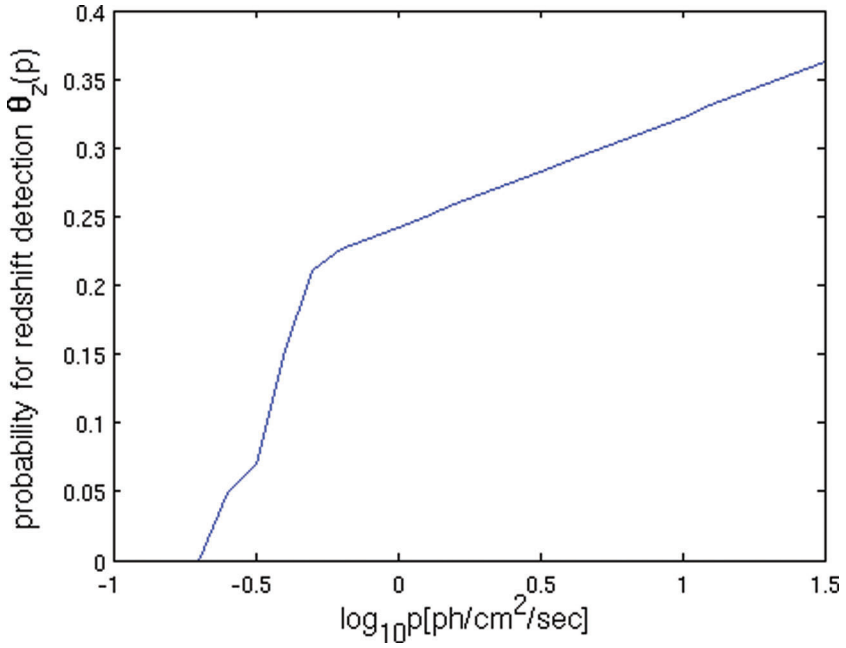

Figure B4. The probability for measuring redshift by absorption lines or by photometry θ_z, as a function of log(peak flux).

B1.1 Redshift measuring probability

Redshifts are measured only for a moderate fraction of the detected bursts. A few (5–10 per cent) are too weak, some do not have a clear redshift signature and some are not measured because of lack of observational resources.

When we consider the fraction of redshift-measured GRBs to the total number of GRBs detected, we see a trend of increase in this fraction with the measured peak number flux of photons in the detectors main band: 15–150 keV, p (see Fig. B2). We used a linear regression to approximate the relation

$$\theta_z(p)/\theta_\gamma(p) = a\log(p) + b\ , \tag{B2}$$

where $\theta_\gamma(p)$ is the detection probability and $\theta_z(p)$ is the probability that a redshift will be measured. The parameters found in fit are $a = 0.080 \pm 0.078$ and $b = 0.242 \pm 0.054$ with $\chi^2 = 1.01$ at 5 d.o.f., giving a rejection probability of 0.038 . We expect the fraction of number of bursts with redshift $N_z(p)$ to the overall number of bursts $N_\gamma(p)$, for any given p, to obey the relation:

$$\frac{\theta_z(p)}{\theta_\gamma(p)} = \frac{N_z(p)}{N_\gamma(p)}\ . \tag{B3}$$

Fig. B2 depicts the fraction of bursts with a measured redshift and the linear fit, for the absorption and photometry redshifts. Although the fit is acceptable, the significant of the effect is just one standard deviation (σ) – so with the current observations, the option of no dependence of redshift detection probability with peak flux ($a = 0$) is still marginally consistent.

Whereas the detection fraction can be fitted well with a linear model for the redshifts obtained using absorption lines, the case is different when considering redshifts obtained using emission lines. Fig. B3 shows the measured redshift fraction and the linear fit for the emission lines redshifts. The emission lines redshifts are obtained preferably for high-flux bursts, but very few are obtained for low and medium fluxes: 24 per cent for $\log_{10} p > 1$ and only 6.5 per cent for $\log_{10} p \leq 1$. This feature of the emission lines redshifts is associated with a strong bias towards lower redshifts as shown in Fig. 1. These results support our approach of selecting only the absorption lines and photometry redshifts as it make a sample, which is less biased and easier to model.

Table B1. Model's best-fitting parameters when taking (+) and when not taking (−) each effect into account.

Prob. z	Prob. γ	$L*$	α	β	z_1	n_1	n_2
−	−	52.54	0.17	1.32	3.13	1.85	−1.38
−	+	52.53	0.04	1.32	2.25	1.53	−0.00
+	−	52.53	0.30	1.44	3.08	2.28	−1.06
+	+	52.53	0.17	1.44	3.11	2.07	−1.36

The product of the above probabilities for burst detection and redshift measurement gives the total probability that we detect a burst and measure its redshift θ_z. Fig. B4 shows the function θ_z, which have the form

$$\theta_z(p) = \begin{cases} [a\log(p)+b]\left[\frac{(1+c)}{2} + \frac{(1-c)}{2}\mathrm{erf}(d\log(p/p_0))\right] & p \geq 0.2, \\ 0 & p < 0.2, \end{cases} \tag{B4}$$

with

$$a = 0.08, b = 0.242, c = 0.25, d = 10, \log_{10} p_0 = -0.42.$$

To check the effects of the burst detection probability and the redshift measurement probability, we repeated the process described in this paper, with all four options of taking or not taking into account each of the modified probabilities. The best-fitting results for the parameters are shown in Table B1. For both corrections, we find a non-negligible effect on the results, although the deviations induced on the parameters are in most cases within the statistical error ranges of the analysis. When taking both effects into account, the models give somewhat better results in the various statistical tests. Therefore, the function $\theta_z(p)$ that takes both effects into account is used in this work.

This paper has been typeset from a TEX/LATEX file prepared by the author.